Facile Fabrication of ZnO/TiO$_2$ Heterogeneous Nanofibres and Their Photocatalytic Behaviour and Mechanism towards Rhodamine B

Regular Paper

JiaDong Chen[1], WeiSha Liao[1], Ying Jiang[1], DanNi Yu[1], MeiLing Zou[1], Han Zhu[1], Ming Zhang[1]* and MingLiang Du[1]

1 Department of Materials Engineering, College of Materials and Textiles, Zhejiang Sci-Tech University, Hangzhou, P. R. China
*Corresponding author(s) E-mail: zhangming@zstu.edu.cn

Abstract

In this study, novel titanium dioxide (TiO$_2$) and zinc oxide (ZnO) hybrid photocatalysts in the form of nanofibres were fabricated by a facile method using electrospinning followed by a calcination process. Scanning electron microscopy (SEM), transmission electron microscopy (TEM), X-ray diffraction (XRD) and X-ray photoelectron spectroscopy (XPS) were employed to investigate the morphology and structure of the heterogeneous nanofibres. The photocatalytic performances were evaluated via the photodegradation of Rhodamine B (RhB) under irradiation with UV light. Due to the low recombination rate of photo-induced charge carriers, the high utilization efficiency of UV light and the large contact area with the target molecules, the ZnO/TiO$_2$ hybrid nanofibres exhibited high catalytic activity towards the Rhodamine B, and the amount of Zn(OAc)$_2$ in the precursor of these nanofibres played an important role in determining the photo decomposition performance.

Keywords Nanofibres, Photocatalytic Activities, Zinc Oxide, Titanium Dioxide, Rhodamine B

1. Introduction

As a result of industrial development, a variety of contaminants have been discharged into water bodies. This has had a negative effect on the environment. Dyes, such as Rhodamine B (RhB), are widely utilized in textile industries due to their stability and bright colour [1]. Microorganisms in water cannot easily degrade most dyes and some of them can generate carcinogenic substances during the decomposition process [2]. Usually, physical and biological methods are not effective in removing dyes from water [3]. In recent years, photodegradation has been considered an efficient method for treating dye-containing sewage [4, 5]. Titanium dioxide (TiO$_2$) has attracted much attention due to its low cost and good photocatalytic activity [6]. TiO$_2$ has three main phases: rutile, anatase and brookite. The anatase form exhibits the best photocatalytic performance due to its low recombination rate of charge carriers [7]. Zinc oxide (ZnO), with a band gap comparable to that of TiO$_2$, also possesses a high photocatalytic performance [8, 9]. However, the band gaps of both ZnO and TiO$_2$ are relatively high, which limits their uses in practical applications. Both TiO$_2$ and

ZnO require a high-energy light source, such as UV light, to generate photo-generated electrons and holes.

So far, research efforts have focused on increasing the ability to harvest light, and many approaches have been employed to modify catalysts. Typical methods are as follows: the synthesis of heterogeneous hybrids consisting of various semiconductors, doping with noble metals and transition metals [10-13]. The resultant hybrids usually exhibit much better catalytic performance than the bare catalysts. To improve the efficiency of the contact with contaminants, catalysts are usually fabricated at the nanoscale. Most ZnO/TiO_2 hybrids are in the form of nanoparticles due to their unique geometries [14, 15]. However, nanoparticles are difficult to recycle from a suspension and may cause secondary pollution [16, 17]. The catalytic performances of nanofibres are superior to those of spherical nanoparticles due to the relatively high specific area and unique nanoparticle alignment. This can cause efficient charge separation through interparticle charge transfer along the nanofibre framework [18]. Therefore, catalysts in the form of nanofibres have attracted much attention. Electrospinning is an efficient way to fabricate nanofibres and various shaped fibres such as hollow tubes, ribbons and filled tubes [19-24].

In this work, ZnO/TiO_2 hybrid nanofibres were prepared via electrospinning to obtain the precursor of hybrid nanofibres. This was followed by calcination in a muffle furnace. The photocatalytic performance of the product was evaluated by analysing the photodegradation of RhB under ultraviolet illumination. The synthesized products possessed high degradation efficiency. The ZnO/TiO_2 (1 wt %) nanofibres degraded 90% of the dyes in about 15 min. In the present work, this is the most effective of the prepared samples.

2. Experimental Materials

Tetrabutyltitanate (TTB), Polyvinyl pyrrolidone (PVP, MW=1,300,000), zinc acetate $(Zn(OAc)_2)$, lithium hydroxide (LiOH) and ethanol (CH_3CH_2OH) were all purchased from Aladdin chemistry Co., Ltd. The RhB dye was obtained from Hangzhou Gaojing Fine Chemical Co., Ltd. All of the reagents were of analytical grade and used without further purification.

2.1 Synthesis of ZnO-ethanol Solution

ZnO solution was obtained via a facile method using ethanol as the solvent. Following the typical procedure, to obtain the homogeneous LiOH solution, 0.87 g lithium hydroxide was added to 75 ml absolute ethanol and the mixture was sonicated for 2 h to promote dissolution. Then, 3.2 g zinc acetate was dissolved in 150 ml absolute ethanol and the suspension was heated to 90 °C under continuous stirring until complete dissolution was achieved. Next, the prepared lithium hydroxide solution was added drop-wise into the zinc acetate solution at ambient temperature under

magnetic stirring for 2 h. Finally, the mixture was magnetically stirred for 30 min after the addition process was completed to obtain the ZnO-ethanol solution.

2.2 Synthesis of the ZnO/TiO₂ Hybrid Nanofibres

Following a typical synthesis method, 1.7 g PVP was added to 14 ml ZnO-ethanol solution under magnetic stirring for 3 h. Then, 3 ml TTB was mixed with the prepared solution following another 3 h of stirring to obtain a homogeneous solution. Next, the precursor was fed to the nozzleless electrospinning device. The conditions of electrospinning were as follows: the distance from the electrode to collector, 12 cm; voltage, 18 kV; and flow rate, 0.5 ml/h. To obtain the ZnO/TiO_2 nanofibres, the resultant spun nanofibres were heated from room temperature to 200 °C at a controlled heating rate of 0.5 °C/min, followed by a constant temperature for 2 h in a muffle furnace. Subsequently, it was continuously heated up to 600 °C and then held for 3 h. Finally, it was left to cool down to room temperature naturally. Other nanofibres containing different amounts of $Zn(OAc)_2$ in the precursor can be synthesized using the same method. Due to the usage of LiOH in the preparation of the ZnO nanoparticles, Li element exists in the form of Li(OAc) after reacting with $Zn(OAc)_2$. Finally, it becomes Li_2O in the sintered nanofibres. Compared to the amount of ZnO and TiO_2, Li_2O is negligible and most of them are embedded in nanofibres. Therefore, it has little influence on the degradation efficiency. In addition, the prepared nanofibres containing different zinc acetate contents of 0.5 wt%, 1 wt% and 2 wt% in the precursor are denoted as ZnO/TiO_2 (0.5 wt%), ZnO/TiO_2 (1 wt%) and ZnO/TiO_2 (2 wt%) nanofibres.

2.3 Photodegradation Experiments

The evaluation of the photodecomposition activity was performed via a Xujiang electromechanical photoreactor. This consists of a 400 W high-pressure mercury lamp, which is placed in the centre of a quartz cold trap. Around the trap, there is a cylinder-like barrel that is filled with flowing cool water. A test tube with a plug used for the storage of the RhB dyes can be set in a fixture with a circular hole between the barrel and cold trap. The tube is submerged into the water, thus keeping the temperature of the contaminant cool enough to avoid the volatilization of RhB. A magnetic stirrer is provided under the reaction tube. In each trial, 3 mg of catalyst was added to 30 ml of 2 ppm RhB dye aqueous solutions. Prior to irradiation, the suspension was magnetically stirred for 30 min to achieve the equilibrium of adsorption and desorption between the catalyst and the dyes in the dark. At given time intervals, 3 ml of the sample was collected from the reactor. Then, the catalyst was eliminated from the suspension by centrifugation. The filtrate was analysed utilizing a UV-Vis spectrophotometer to determine the concentration of the RhB dye solution.

3. Results and Discussion

3.1 Morphologies and Structures of the ZnO/TiO_2 Heterogeneous Nanofibres

SEM analysis was carried out to investigate the morphologies of the obtained hybrid nanofibres before and after calcination. Compared to PVP-TTB nanofibres, the $Zn(OAc)_2$-PVP-TTB nanofibres with different amounts of $Zn(OAc)_2$ were randomly distributed, accompanying a relatively smooth surface, depending on the amorphous character of the nanofibres. Moreover, an increase of the $Zn(OAc)_2$ content in the precursor produced belt-like nanofibres, as can be clearly seen in Fig. 1 (d). This phenomenon may be attributed to the hydrolysis of TTB. The diameter of the precursor of hybrid nanofibres also slightly increased. After calcination, the nanofibres decreased in diameter due to the elimination of water and organics. Meanwhile, the surface of these fibres was relatively rough because of the formation of nanoparticles on it. However, the overall morphology, such as the reticular conformation, remained. At the same calcination temperature, the ZnO/TiO_2 (1 wt%) nanofibres possessed more fractured surfaces existing as loose ends. These enhanced the surface area and improved the contact area with the contaminants during photodegradation. Therefore, the photodegradation efficiency of the ZnO/TiO_2 (1 wt%) nanofibres was higher than that of the other nanofibres. In addition, an element analysis of the photocatalysts was carried out using an energy-dispersive X-ray spectrometer (EDX) attached to the scanning electron microscope, as shown in Fig. 2. This shows that the obtained nanofibres were composed of carbon, titanium, zinc and oxygen elements. Therefore, the EDX results demonstrate the coexistence of ZnO and TiO_2 in the samples. No lithium element was detected from the EDX analysis, indicating negligible content of Li element in the sample. The molar ratio of Ti to Zn was about 5.1, showing a large proportion of TiO_2 in the sample. It can also be seen that there was only a little carbon element in the nanofibre, indicating the decomposition of almost all of the PVP.
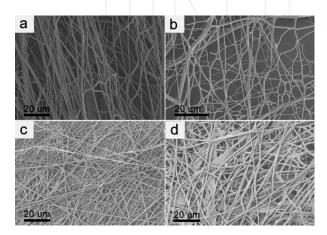

Figure 2. SEM pictures of the pure TiO_2 and the ZnO/TiO_2 nanofibres with different content of $Zn(OAc)_2$ in the precursor after calcination: (a) bare TiO_2, (b) 0.5 wt%, (c) 1 wt%, (d) 2 wt%, (e) SEM image of ZnO/TiO_2 (1 wt%) nanofibres, (f) EDX spectra from the selected region in image E

TEM analysis was carried out to further investigate the morphology and crystalline structure. As seen in Fig. 3, the nanofibres were made up of densely packed nanocrystals. Compared with nanoparticles, nanofibres have large specific areas, increasing the active sites and facilitating the adsorption of more contaminants [18]. As shown in Fig. 3(a-d), the diameter of the samples also increased with increasing amounts of $Zn(OAc)_2$ in the precursor, which is consistent with the results from the SEM observation. In addition, the fibrous appearance of the hybrid was unaltered after calcination.

Figure 3. TEM images of TiO_2 and ZnO/TiO_2 nanofibres containing different amounts of $Zn(OAc)_2$ in the precursor: (a) TiO_2 (b) 0.5 wt%, (c) 1 wt%, (d) 2 wt%

To verify the crystal structure of the heterogeneous nanofibres, XRD analysis was conducted. Fig. 4 exhibits the XRD patterns of the ZnO-PVP-TTB fibre, pure TiO_2 and the

Figure 1. SEM images of PVP-TTB and $Zn(OAc)_2$-PVP-TTB nanofibres with different content of zinc acetate: (a) PVP-TTB, (b) 0.5 wt%, (c) 1 wt%, (d) 2 wt%
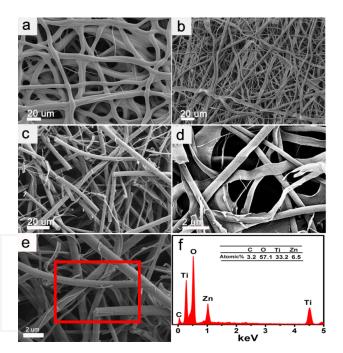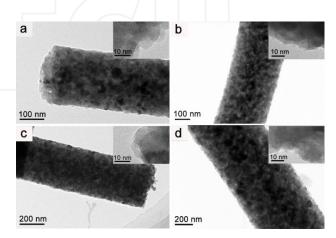
ZnO/TiO$_2$ nanofibres with different Zn(OAc)$_2$ content in the precursor. It is well known that TiO$_2$ mainly possesses the two crystalline phases of anatase and rutile, denoted as (A) and (R), respectively. The typical peaks of TiO$_2$ located at 2θ = 24.8° and 27.1° are ascribed to the (101) plane of anatase and the (110) phase of rutile, respectively. It could be seen that pure TiO$_2$ nanofibres were mainly composed of the rutile phase. However, the intensity of the anatase A (101) enhanced whilst the Zn(OAc)$_2$ content in the precursor was increased, showing the increased anatase phase of TiO$_2$ in the nanofibre. The ZnO phase emerged when Zn(OAc)$_2$ was added to the precursor. In addition, ZnO-PVP-TTB did not show any well-defined peaks, while the peak of the ZnO/TiO$_2$ nanofibres was distinct, suggesting that the nanofibres exhibit good crystallinity after calcination.
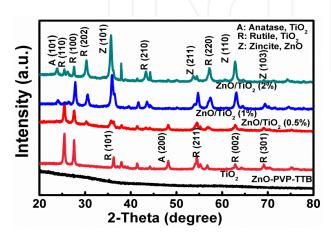

Figure 4. XRD patterns of ZnO-PVP-TTB, TiO$_2$ and ZnO/TiO$_2$ nanofibres with different content of Zn(OAc)$_2$ in the precursor

XPS analysis was conducted to study the chemical states of the prepared nanofibres. As shown in Fig. 5, the XPS spectrum of Zn 2p had two peaks located at 1044.7 eV and 1020.7 eV, which is ascribed to Zn 2p$_{1/2}$ and 2p$_{3/2}$, respectively. This demonstrates the presence of Zn^{2+} in the sample. Furthermore, the Ti 2p peak of the ZnO/TiO$_2$ (1 wt %) nanofibres emerged at 464.3 eV and 458.5 eV, which can be ascribed to Ti 2p$_{1/2}$ and 2p$_{3/2}$, respectively. This also confirms the appearance of Ti^{4+} in the sample. Therefore, the XPS images further verify the coexistence of TiO$_2$ and ZnO in the product. In addition, the binding energy of Li 1s was 55.56 eV, which confirms the presence of Li$_2$O. In the EDX analysis, Li element was not detected, suggesting the negligible content of Li.

The diffuse reflectance UV-Vis spectra of both ZnO/TiO$_2$ (1 wt%) and TiO$_2$ nanofibres are shown in Fig. 6. It can be seen from the absorption spectra that the absorption edge of ZnO/TiO$_2$ (1 wt%) had a red shift. To calculate the band gaps, Kubelka-Munk equation was employed. The band gaps of ZnO/TiO$_2$ (1 wt%) and TiO$_2$ nanofibres were determined to be 2.8 eV and 3.1 eV, respectively. The band gap energy of the ZnO/TiO$_2$ (1 wt%) nanofibres decreased due to the synergistic effect between the conduction band of TiO$_2$ and that of ZnO. Both impurity and defect levels
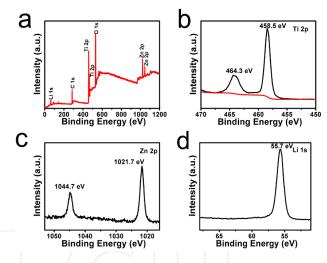

Figure 5. XPS spectra of ZnO/TiO$_2$ (1 wt%) hybrid: (a) survey, (b) Ti 2p peak, (c) Zn 2p peak, (d) Li 1s peak

were introduced to the forbidden band of TiO$_2$ due to the formation of some sub-bands. Thus, the band gap energy reduced [25-27]. The principle of the synergistic effect between ZnO and TiO$_2$ is illustrated in Fig. 10.
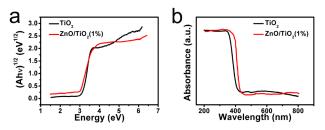

Figure 6. (a) DRS of TiO$_2$ and ZnO/TiO$_2$ (1wt%) nanofibres. Data are plotted as transformed Kubelka-Munk function versus the energy of light, (b) the absorption spectra between 200 and 800 nm.

3.2 Photocatalytic Activities and the Kinetics Model of the ZnO/TiO$_2$ Nanofibres

As the RhB molecular was very stable and the bleaching under UV light irradiation was insignificant during the degradation process, the photocatalytic performances of pure TiO$_2$ and the ZnO/TiO$_2$ nanofibres were evaluated using RhB as a target probe molecule. The results are shown in Fig. 7. Following 15 min of exposure to UV light, the photo catalytic efficiencies of TiO$_2$, ZnO/TiO$_2$ (0.5 wt%), ZnO/TiO$_2$ (1 wt%), and ZnO/TiO$_2$ (2 wt%) nanofibres were 57.06%, 81.73%, 92.57% and 47.90%, respectively. It is worth noting that the ZnO/TiO$_2$ (1 wt%) hybrids possessed the highest decomposition efficiency at 92.57%. Whilst the Zn(OAc)$_2$ content in the precursor of the nanofibres was increased, the photodegradation activity significantly increased as well. However, the efficiency remarkably decreased to values that were even lower than for pure TiO$_2$ when the zinc acetate content in the precursor reached 2 wt%. The anatase phase of TiO$_2$ absorbed more UV light than the rutile structure. Furthermore, when the amount of

Zn(OAc)$_2$ content in the precursor increased to an acceptable range, the anatase ratio was enhanced, as shown in the XRD patterns, thus promoting the trapping of UV light and increasing the photocatalytic performance. At the same time, ZnO acted as a co-catalyst and decreased the recombination of the charge carriers. However, when the amount of zinc acetate increased to 2 wt%, ZnO could have been excessive, and it is likely that too many holes accumulated on the conduction band. Therefore, superfluous charge carriers could not be consumed instantaneously, and excessive ZnO may have acted as recombination centres for electrons and holes. In this case, the doping of ZnO could improve the proportion of anatase phases and generate many charge carriers by enhancing the absorption of UV light in TiO$_2$, which is consistent with the XRD analysis results. However, the total number of separated charge carriers declined after balancing the two opposite effects. Thus, superfluous Zn(OAc)$_2$ led to poorer photodegradation performances for the ZnO/TiO$_2$ (2 wt%) nanofibres compared to the pure TiO$_2$ nanofibres. The reason for the decrease in the photo activity with increasing Zn(OAc)$_2$ content to 2 wt% is as follows: the doping of a large amount of ZnO remarkably decreased the total number of separated electrons-holes.

Figure 8. Absorption spectral changes of RhB under UV light illumination (ZnO/TiO$_2$ (1 wt%)

The degradation process of RhB was analysed via the establishment of the Langmuir-Hinshelwood model [28-30]. The relevant equations are expressed as follows:

$$r_t = -\frac{dC_t}{dt} = \frac{k_r K_1 C_t}{K_2 C_{st} + K_1 C_t + 1} \tag{1}$$

$$r_t = -\frac{dC_t}{dt} = \frac{k_r K_1 C_t}{K_1 C_t + 1} \tag{2}$$

$$r_t = -\frac{dC_t}{dt} = k_r K_1 c_t = K c_t \tag{3}$$

$$-\int_{c_0}^{c_t} \frac{1}{c_t} dt = \int_0^t K dt \tag{4}$$

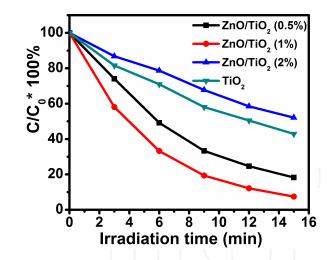$$\ln \frac{c_0}{c_t} = Kt. \tag{5}$$

Figure 7. The photocatalytic performance of the sample for RhB degradation

The temporal concentrations of the solution at different given times were estimated by the UV-Vis absorbance at about 554 nm, which corresponds with the typical maximum absorption wavelength of RhB. Fig. 8 shows the function of UV-Vis light absorbance versus time and it can be seen that the absorption intensity gradually declined as time went on, indicating the gradual degradation of the contaminant. The location of the maximum adsorption peak remained unchanged during the analysis process, suggesting that there were no impurities in the analysed solution. Moreover, the colour of the RhB solution changed from pink to almost colourless during the entire degradation process over approximately 15 min of illumination time, implying the reducing concentration of RhB.
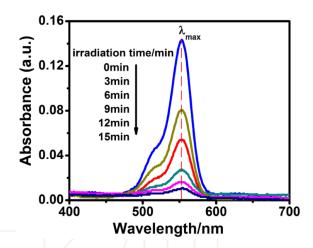
In eq(1), r_t is the reaction rate, c_t is the concentration of the RhB dyes at time t, k_r is the reaction rate constant, K_1 is the coefficient of adsorption of the RhB dyes, K_2 is the adsorption coefficient of dissolvent and c_{st} is the concentration of the solvent at time t. Compared with the reactant, the adsorption of the dissolvent is negligible. Hence, eq(1) can be expressed as eq(2). Meanwhile, the concentration of the dyes is extremely low and $K_1 C_t$ is much lower than 1. Therefore, eq(2) can be further simplified to eq(3), where K is the product of k_r and K_1 and is also a constant. As shown in eq(4), the final kinetic model (eq(5)) can be obtained by computing the integral of eq(3). As seen in eq(5), the constant K represents the efficiency in the degradation of the RhB dyes. The kinetic curves and the relevant constants (K) are shown in Fig. 9 and Table 1. The reaction rate constant (K) was 0.0550, 0.1161, 0.1736 and 0.0437 min^{-1} for

the $Zn(OAc)_2$ amounts in the precursor of 0, 0.5 wt%, 1 wt %, and 2 wt%, respectively. The K value of the ZnO/TiO_2 (1 wt%) nanofibres was the highest among these samples, suggesting that the degradation efficiency of the ZnO/TiO_2 (1wt%) nanofibres was higher than that of other nanofibres. From the result, it can be said that the amount of $Zn(OAc)_2$ content in the precursor of the nanofibres played a vital role in the degradation process of the RhB dyes. When the $Zn(OAc)_2$ content in the precursor of the sample was increased, the removal efficiency also increased, which could be attributed to the enhanced synergistic effect between ZnO and TiO_2. Meanwhile, an excessive amount of $Zn(OAc)_2$ content in the precursor caused a decrease in the K value. This is because superfluous ZnO possibly became recombination centres, thus reducing the separation efficiency of photo-generated electrons and holes.
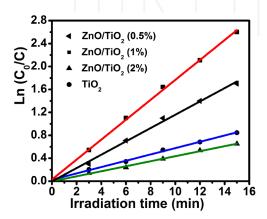

Figure 9. Fitting curves of the kinetic model for various nanofibres

Samples	Photo Catalyst	Kinetic Equation	K(min⁻¹)	R²
1	TiO_2	$\ln(C_0/C)=0.0550t$	0.0550	0.998
2	ZnO/TiO_2 (0.5%)	$\ln(C_0/C)=0.1161t$	0.1161	0.996
3	ZnO/TiO_2 (1%)	$\ln(C_0/C)=0.1736t$	0.1736	0.998
4	ZnO/TiO_2 (2%)	$\ln(C_0/C)=0.0437t$	0.0437	0.997

Table 1. The kinetic equations, rate constants (k) and regression coefficients (R^2) of photocatalytic degradation of RhB for various samples

3.3 Photocatalytic Mechanism

Based on the above results, a possible mechanism proposed for the degradation of the RhB dyes by ZnO/TiO_2 nanofibres is shown in Fig. 10. The improved activity in the photodegradation could be attributed to the enhanced separation efficiency of charge carriers resulting from the charge transfer between ZnO and TiO_2. The charge carriers were generated simultaneously via the excitation by UV illumination and gathered on the conduction and valance bands of ZnO and TiO_2, respectively. Without doping with ZnO, the photo-induced electrons and holes generated from TiO_2 could quickly recombine with each other, thus resulting in reduced photo catalytic performance. After the introduction of ZnO, some sub-bands were formed by introducing both defect levels and impurities into the forbidden band, which resulted in a decrease in the energy gap. Additionally, the ability of the ZnO/TiO_2 nanofibres to harvest UV light was improved due to the decrease in the band gap of TiO_2 [25-27]. Furthermore, due to the synergistic effects between ZnO and TiO_2, the recombination rate of the charge carriers was suppressed. Thus, more electrons and holes were available to decompose the contaminants and enhance the photo catalytic efficiency. Moreover, photo-induced electrons are mainly consumed in two ways: the first is the reaction with H_2O and O_2 adsorbed on the surface of the catalysts, resulting in the production of some radicals and negative ions [31, 32]. The second is the combination with dissolved O_2 in water, leading to the consumption of electrons to promote the separation process [33, 34]. As described above, the electrons from the ZnO and holes from the TiO_2 could transfer to the corresponding bands of the counterpart and also facilitate the separation of charge carriers. After introducing ZnO to TiO_2, the separation efficiency substantially increased. Thus, the photo catalytic activities significantly improved.
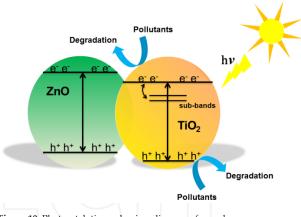

Figure 10. Photocatalytic mechanism diagram of samples

4. Conclusions

In summary, ZnO/TiO_2 photo catalysts were synthesized successfully and exhibited excellent photocatalytic performances in the decomposition of RhB dyes. The amount of $Zn(OAc)_2$ content in the precursor of nanofibres heavily influenced the photodegradation activities and diameters of the prepared nanofibres. The optimum content of zinc acetate in the precursor was found to be 1 wt%. The optimum photo-decomposition activities are attributed to the low recombination rate of the photo-generated charge carriers, the high utilization of ultraviolet light and the large contact area with contaminants. This work provides a potential photocatalyst for the degradation of contaminants and a facile way to prepare a recyclable photocatalyst.

5. Acknowledgements

6. References

[1] Bauer C, Jacques P, Kalt A (2001) Photooxidation of an Azo Dye Induced by Visible Light Incident on the Surface of TiO_2. Journal of Photochemistry and Photobiology A: Chemistry 140:87-92.

[2] Horikoshi S, Hojo F, Hidaka H, Serpone N (2004) Environmental Remediation by an Integrated Microwave/UV Illumination Technique. 8. Fate of Carboxylic Acids, Aldehydes, Alkoxycarbonyl and Phenolic Substrates in a Microwave Radiation Field in the Presence of TiO_2 Particles under UV Irradiation. Environmental Science & Technology 38:2198-2208.

[3] Kyung H, Lee J, Choi W (2005) Simultaneous and Synergistic Conversion of Dyes and Heavy Metal Ions in Aqueous TiO_2 Suspensions Under Visible-light Illumination. Environmental Science & Technology 39:2376-2382.

[4] Arslan I, Balcioglu IA, Bahnemann D W (2000) Heterogeneous Photocatalytic Treatment of Simulated Dyehouse Effluents Using Novel TiO_2-photocatalysts. Applied Catalysis B: Environmental 26:193-206.

[5] Vinodgopal K, Wynkoop D E, Kamat P V (1996) Environmental Photochemistry on Semiconductor Surfaces: Photosensitized Degradation of a Textile Azo Dye, Acid Orange 7, on TiO_2 Particles Using Visible Light. Environmental Science & Technology 30:1660-1666.

[6] Carp O, Huisman C L, Reller A (2004) Photoinduced Reactivity of Titanium Dioxide. Progress in Solid State Chemistry 32:33-177.

[7] Chorfi H, Saadoun M, Bousselmi L, Bessais B (2012) TiO_2-ITO and TiO_2-ZnO Nanocomposites: Application on Water Treatment. EPJ Web of Conferences 29:00015.

[8] Lai Y, Meng M, Yu Y, Wang X, Ding T (2011) Photoluminescence and Photocatalysis of the Flower-like Nano-ZnO Photocatalysts Prepared by a Facile Hydrothermal Method with or Without Ultrasonic Assistance. Applied Catalysis B: Environmental 105:335-345.

[9] Wan Q, Wang T H, Zhao J C (2005) Enhanced Photocatalytic Activity of ZnO Nanotetrapods. Applied Physics Letters 87:083105.

[10] Labiadh H, Chaabane T B, Balan L, Becheik N, Corbel S, Medjahdi G, Schneider R (2014) Preparation of Cu-doped ZnS QDs/TiO_2 Nanocomposites with High Photocatalytic Activity. Applied Catalysis B: Environmental 144:29-35.

[11] Achouri F, Corbel S, Aboulaich A, Balan L, Ghrabi A, Ben Said M, Schneider R (2014) Aqueous Synthesis and Enhanced Photocatalytic Activity of ZnO/Fe_2O_3 Heterostructures. Journal of Physics and Chemistry of Solids 75:1081-1087.

[12] Conesa J C (2013) Band Structures and Nitrogen Doping Effects in Zinc Titanate Photocatalysts. Catalysis Today 208:11-18.

[13] Wang D, Zhou Z-H, Yang H, Shen K-B, Huang Y, Shen S (2012) Preparation of TiO_2 Loaded with Crystalline Nano Ag by a One-step Low-temperature Hydrothermal Method. Journal of Materials Chemistry 22:16306-16311.

[14] Liu G, Li G, Qiu X, Li L (2009) Synthesis of ZnO/titanate Nanocomposites with Highly Photocatalytic Activity Under Visible Light Irradiation. Journal of Alloys and Compounds 481:492-497.

[15] Azouani R, Michau A, Hassouni K, Chhor K, Bocquet J F, Vignes J L, Kanaev A (2010) Elaboration of Pure and Doped TiO_2 Nanoparticles in Sol–gel Reactor with Turbulent Micromixing: Application to Nanocoatings and Photocatalysis. Chemical Engineering Research and Design 88:1123-1130.

[16] Bakhtari K, Guldiken R O, Makaram P, Busnaina A A, Park J-G (2006) Experimental and Numerical Investigation of Nanoparticle Removal Using Acoustic Streaming and the Effect of Time. Journal of The Electrochemical Society 153:G846-G850.

[17] Dreher K L (2004) Health and Environmental Impact of Nanotechnology: Toxicological Assessment of Manufactured Nanoparticles. Toxicological Sciences 77:3-5.

[18] Choi S K, Kim S, Lim S K, Park H (2010) Photocatalytic Comparison of TiO_2 Nanoparticles and Electrospun TiO_2 Nanofibers: Effects of Mesoporosity and Interparticle Charge Transfer. The Journal of Physical Chemistry C 114:16475-16480.

[19] Bashouti M, Salalha W, Brumer M, Zussman E, Lifshitz E (2006) Alignment of Colloidal CdS Nanowires Embedded in Polymer Nanofibers by Electrospinning. ChemPhysChem 7:102-106.

[20] Li D, Xia Y (2004) Electrospinning of Nanofibers: Reinventing the Wheel? Advanced Materials 16:1151-1170.

[21] Sun Y, Mayers B, Xia Y (2003) Metal Nanostructures with Hollow Interiors. Advanced Materials 15:641-646.

[22] Kim T W, Hwang S J, Jhung S H, Chang J S, Park H, Choi W, Choy J H (2008) Bifunctional Heterogeneous Catalysts for Selective Epoxidation and Visible

Light Driven Photolysis: Nickel Oxide-containing Porous Nanocomposite. Advanced Materials 20:539-542.

[23] Marcì G, Augugliaro V, López-Muñoz M J, Martín C, Palmisano L, Rives V, Schiavello M, Tilley R J D, Venezia A M (2001) Preparation Characterization and Photocatalytic Activity of Polycrystalline ZnO/TiO$_2$ Systems. 2. Surface, Bulk Characterization, and 4-Nitrophenol Photodegradation in Liquid–solid Regime. The Journal of Physical Chemistry B 105:1033-1040.

[24] Kostedt, Ismail A A, Mazyck D W (2008) Impact of Heat Treatment and Composition of ZnO–TiO$_2$ Nanoparticles for Photocatalytic Oxidation of an Azo Dye. Industrial & Engineering Chemistry Research 47:1483-1487.

[25] Pei C C, Leung W W-F (2013) Photocatalytic Degradation of Rhodamine B by TiO$_2$/ZnO Nanofibers Under Visible-light Irradiation. Separation and Purification Technology 114:108-116.

[26] Perkgoz N K, Toru R S, Unal E, Sefunc M A, Tek S, Mutlugun E, Soganci I M, Celiker H, Celiker G, Demir H V (2011) Photocatalytic Hybrid Nanocomposites of Metal Oxide Nanoparticles Enhanced Towards the Visible Spectral Range. Applied Catalysis B: Environmental 105:77-85.

[27] Štengl V, Bakardjieva S, Murafa N (2009) Preparation and Photocatalytic Activity of Rare Earth Doped TiO$_2$ Nanoparticles. Materials Chemistry and Physics 114:217-226.

[28] Li Y, Li X, Li J, Yin J (2006) Photocatalytic Degradation of Methyl Orange by TiO$_2$-coated Activated Carbon and Kinetic Study. Water Research 40:1119-1126.

[29] Sun J, Wang X, Sun J, Sun R, Sun S, Qiao L (2006) Photocatalytic Degradation and Kinetics of Orange G Using Nano-sized Sn(IV)/TiO$_2$/AC Photocatalyst. Journal of Molecular Catalysis A: Chemical 260:241-246.

[30] Wu C-H, Chang H-W, Chern J-M (2006) Basic Dye Decomposition Kinetics in a Photocatalytic Slurry Reactor. Journal of Hazardous Materials 137:336-343.

[31] Wang Q, Yun G, Bai Y, An N, Lian J, Huang H, Su B (2014) Photodegradation of Rhodamine B with MoS$_2$/Bi$_2$O$_2$CO$_3$ Composites Under UV Light Irradiation. Applied Surface Science 313:537-544.

[32] Zheng Y, Duan F, Chen M, Xie Y (2010) Synthetic Bi$_2$O$_2$CO$_3$ Nanostructures: Novel Photocatalyst with Controlled Special Surface Exposed. Journal of Molecular Catalysis A: Chemical 317:34-40.

[33] Xiang Q, Yu J, Jaroniec M (2012) Graphene-based Semiconductor Photocatalysts. Chemical Society Reviews 41:782-796.

[34] Liu J, Bai H, Wang Y, Liu Z, Zhang X, Sun D D (2010) Self-assembling TiO$_2$ Nanorods on Large Graphene Oxide Sheets at a Two-phase Interface and Their Anti-recombination in Photocatalytic Applications. Advanced Functional Materials 20:4175-4181.